PNAS RESEARCH ARTICLE | CELL BIOLOGY

Selective targeting of metastatic ovarian cancer using an engineered anthrax prodrug activated by membrane-anchored serine proteases

Nadire Duru[a,b,1], Nisha R. Pawar[a,b,1], Erik W. Martin[a,b], Marguerite S. Buzza[a,b,c], Gregory D. Conway[a,b], Rena G. Lapidus[c], Shihui Liu[d], Jocelyn Reader[c,e], Gautam G. Rao[c,e], Dana M. Roque[c,e], Stephen H. Leppla[d], and Toni M. Antalis[a,b,c,f,2]

Edited by Robert Collier, Harvard Medical School, Boston, MA; received January 25, 2022; accepted May 5, 2022

Treatments for advanced and recurrent ovarian cancer remain a challenge due to a lack of potent, selective, and effective therapeutics. Here, we developed the basis for a transformative anticancer strategy based on anthrax toxin that has been engineered to be selectively activated by the catalytic power of zymogen-activating proteases on the surface of malignant tumor cells to induce cell death. Exposure to the engineered toxin is cytotoxic to ovarian tumor cell lines and ovarian tumor spheroids derived from patient ascites. Preclinical studies demonstrate that toxin treatment induces tumor regression in several in vivo ovarian cancer models, including patient-derived xenografts, without adverse side effects, supportive of progression toward clinical evaluation. These data lay the groundwork for developing therapeutics for treating women with late-stage and recurrent ovarian cancers, utilizing a mechanism distinct from current anticancer therapies.

metastatic ovarian cancer | ascites | prodrug | anthrax toxin | membrane-anchored serine proteases

Significance

Ovarian cancer is the most lethal gynecological cancer. Clinically approved chemotherapies aim to slow or stop tumor growth; however, cancer cells continue to evolve between chemotherapy cycles, acquiring properties that allow cell survival and successful dissemination, subsequently developing into life-threatening metastatic tumors. There is an urgent need to develop more effective therapeutic strategies based on the biology of disseminated and metastatic ovarian tumors to achieve long-term remission. Here, we leveraged tumor-associated overactive membrane-anchored serine proteases to develop a potent therapeutic agent that selectively kills ovarian tumor cells by inactivation of pathways that promote tumor cell survival. Clinical translation of these preclinical findings could be an effective therapeutic strategy to improve the prognosis for women with late-stage ovarian cancer.

The prognosis for advanced ovarian cancer (OvCa) is poor due to late-stage disease presentation, early and passive metastasis, and resistance to conventional therapies (1). Despite initial good responses to first-line debulking surgery and platinum/taxane combination chemotherapy, complications resulting from disseminated peritoneal metastasis still cause high patient mortality. Recently, PARP inhibitors have become standard of care after chemotherapy as a first-line maintenance treatment for OvCa patients regardless of their *BRCA* mutation status (2); however, resistance to PARP inhibitors remains a major clinical challenge. Antiangiogenic agents such as bevacizumab, which target tumor-associated vasculature, are utilized in the treatment of OvCa; however, no significant overall survival benefit is achieved for newly diagnosed (3) or recurrent patients (4) treated with concurrent bevacuzimab compared to chemotherapy alone. More effective therapeutic strategies based on the unique biology of metastatic OvCa tumors are needed to achieve long-term cancer remission.

OvCa originates on the surface epithelium of the ovary or the distal fallopian tube (1) and presents as a collection of histological subtypes. Metastasis occurs predominantly by passive transcoelomic dissemination into the peritoneal cavity, with metastasis via hematogenous or lymphatic routes being less common (5, 6). Ascites fluid often accumulates in the peritoneal cavity, further promoting metastatic dissemination. In malignant ascites fluid, tumors can exist as single cells or spheroids that are capable of anchoring to the mesothelial lining, invading the underlying tissues, and establishing foci in surrounding peritoneal organs (5).

Metastatic tumors have long been associated with dysregulated protease activities (7, 8). This association is strongly supported by recent preclinical imaging data demonstrating tumor-associated protease activity in vivo (9–12). Notably, the overactivity of membrane-anchored serine proteases (MASPs) is correlated with advanced stages of OvCa (7), where they can impact detachment from the primary tumor, aggregation and survival in the peritoneal fluid, interaction with the peritoneal lining, invasion to metastatic sites, and angiogenesis (7). MASPs contain a conserved serine protease domain (SPD) required for catalytic activity and either type I or type II transmembrane domains or glycophosphatidylinositol (GPI) anchors that tether the extracellular SPD directly to the cell surface, enabling direct access to the cell surface and pericellular substrates (13, 14). Importantly, MASP proteolytic activity in healthy tissues is transient, with activities tightly regulated by multilayered networks of activators, cofactors, and inhibitors (13). In contrast, constitutive or unrestricted MASP catalytic activities are functionally associated with tumor growth and malignancy (7, 15).

MASPs are synthesized and expressed on the cell surface as inactive precursors, or zymogens, that require activation by pericellular proteases in the tumor microenvironment. Zymogen activation occurs by proteolytic cleavage after an arginine or lysine amino acid

Competing interest statement: Portions of this work are included in US Patent Numbers 10,568,929 and 11,013,784 (E.W.M. and T.M.A.). The authors declare no other potential conflicts of interest.

This article is a PNAS Direct Submission.

See online for related content such as Commentaries.

[1]N.D. and N.R.P. contributed equally to this work.

[2]To whom correspondence may be addressed. Email: tantalis@som.umaryland.edu.

This article contains supporting information online at http://www.pnas.org/lookup/suppl/doi:10.1073/pnas.2201423119/-/DCSupplemental.

Published July 8, 2022.

residue, which is positioned in a conserved activation motif within the MASP catalytic SPD (13). The overactivity of tumor-associated MASPs implies an abundance of zymogen-activating pericellular proteases in the tumor microenvironment. Since MASPs have substrate specificity for cleavage after arginine or lysine residues, several MASPs can activate other MASPs present on the cell surface (13), potentially presenting multiple unique targets for antitumor therapeutic intervention.

Here, we describe the development of zymogen activation prodrug toxins (ZMTs) designed to undergo activation cleavage by zymogen-activating proteases on the tumor cell surface, using a reengineered anthrax toxin (AT) for drug delivery. The AT delivery system is a well-studied two-component system based on *Bacillus anthracis* that utilizes cell surface binding to deliver a potent cytotoxin to cells (16). The mechanism of action requires one component, protective antigen (PA), to bind and undergo activation proteolytic cleavage on the cell surface, initiating oligomerization and formation of a cell-surface pore that allows translocation of the second component, a cytotoxic cargo, into cells (Fig. 1*A*). The natural AT cargo lethal factor (LF) is a zinc-dependent metalloproteinase that irreversibly inactivates mitogen-activated protein kinase kinases (MEKs) and inhibits the oncogenic prosurvival mitogen-activated protein kinase (MAPK) pathway (24, 25) to induce cell death. Another cargo, FP59, is a fusion of the amino-terminal PA-binding domain of LF (amino acids 1 to 254) with the catalytic domain of *Pseudomonas aeruginosa* exotoxin A, which kills cells by adenosine 5′-diphosphate (ADP) ribosylating eukaryotic elongation factor-2 (eEF) and inhibiting protein synthesis (17, 26, 27). Proteolytic cleavage and activation of native PA protein is catalyzed by furin protease. To generate ZMTs, we converted the eight–amino acid furin activation sequence of PA to the zymogen activation sequences corresponding to the MASPs prostasin and testisin and the membrane-associated protease urokinase plasminogen activator (uPA).

We found that PAS, the ZMT with an activation cleavage site mimicking the prostasin zymogen activation site, is a potent substrate for overactive MASPs and functions as a potent tumoricidal prodrug in combination with LF. The PAS:LF toxin is cytotoxic to both ovarian tumor cell lines and tumor cells derived from patient ascites. Preclinical studies using several OvCa xenograft models and an OvCa patient-derived xenograft (PDX) model demonstrate that treatment with PAS:LF toxin significantly reduces tumor burden and extends survival with no evidence of off-target toxicity. This PAS:LF prodrug represents a promising strategy to improve outcomes for women with OvCa.

Results

Generation and Characterization of Reengineered Zymogen Activation Site Toxins. To generate ZMTs predicted to be activated by the overactive MASPs, the P4-P4′ sequence targeted by furin on the native PA (PA-WT; amino acids 164 to 171) (28) was mutated to sequences derived from the prostasin zymogen activation site (PAS), the testisin zymogen activation site (TAS) and the uPA-like zymogen activation site (UAS) (Fig. 1*B*). Prostasin and testisin are GPI-anchored serine proteases that do not self-activate. The pro-prostasin and pro-uPA zymogens are reported substrates for the OvCa-associated MASPs matriptase and hepsin (13). There are no known proteases that cleave the pro-testisin zymogen.

Abrogation of furin-mediated cleavage of the ZMTs was confirmed by incubation of purified PA-WT and recombinant UAS, TAS, and PAS with soluble furin (Fig. 1*C*). PA-WT showed cleavage of the 83-kDa form to the 63-kDa activated form, whereas UAS, TAS, and PAS were resistant to cleavage. Incubation of PA-WT, PAS, UAS, and TAS with recombinant testisin, matriptase, hepsin, and prostasin catalytic domains showed that UAS was only cleaved by testisin and hepsin, while TAS was not cleaved by any of the recombinant MASPs (Fig. 1*D*). Prostasin was unable to cleave PA-WT or any of the ZMTs. PAS was the only ZMT that was able to be cleaved by all three MASPs—testisin, matriptase, and hepsin (Fig. 1*D*). Time course assessment of PAS protein cleavage by recombinant MASPs showed complete activation cleavage of PAS by hepsin within 15 min and less efficient cleavage of PAS by testisin and matriptase (*SI Appendix*, Fig. S1*A*). PAS was not cleaved by recombinant MMP-2/-9 or uPA (Fig. 1*E*), indicating specificity for MASPs. Overactivities of hepsin, matriptase, and testisin have been implicated in OvCa malignancies (7); therefore, we focused on PAS for subsequent in vitro and in vivo studies.

PAS Toxin Is Cytotoxic to Cells Expressing Active MASPs. To investigate effective proteolytic cleavage of PAS on cells by MASP activation, HEK293T cells overexpressing active MASPs (*SI Appendix*, Fig. S1*B–C*) were treated with PAS and the cytotoxic LF-fusion cargo FP59 (26), and viability was assessed by 3-(4,5-dimethylthiazol-2-yl)-2,5-diphenyl-2H-tetrazolium bromide (MTT) assay. Only a few molecules of FP59 are sufficient to inactivate all eEF2 in a cell and inhibit protein synthesis (17); thus, potent cell death is a valuable measurement of PAS activation in vitro. Increasing concentrations of PAS:FP59 resulted in increased dose-dependent cell death for cells expressing hepsin (half-maximal effective concentration, 50% [EC_{50}], 27 ng/mL), testisin (EC_{50}, 22 ng/mL), and matriptase (EC_{50}, 147 ng/mL) compared with control cells (EC_{50} > 500 ng/mL) (*SI Appendix*, Fig. S1*D*). The dependence of cytotoxicity on active testisin was further demonstrated using HEK293T cells stably expressing wild-type testisin (Test) and two catalytically inactive testisin mutants, RA-Test and SA-Test (29). When SA-Test or RA-Test cells were incubated with increasing concentrations of PAS:FP59, viability was similar to that of HEK293T cells expressing the vector alone control (EC_{50} > 500 ng/mL), whereas Test cells were sensitive to PAS:FP59 (EC_{50} < 8 ng/mL) (Fig. 1*F*), strengthening the notion that PAS-induced cytotoxicity is dependent on MASP catalytic activity.

Overactive MASPs in a Broad Range of Human OvCa Cells. MASP expression was investigated using a panel of five high grade serous carcinoma cell lines: ES-2, NCI/ADR-Res, OVCAR3, CAOV3, and COV362 (30,31), in addition to the nontumorigenic IOSE397 cell line derived from immortalized ovarian surface epithelial cells. qPCR analysis revealed that each of the cell lines expressed hepsin, testisin, and matriptase, providing the means for PAS proteolytic activation (Fig. 2*A*). In addition, the cell lines all expressed hepatocyte growth factor activator inhibitors, HAI-1 and HAI-2, cofactors that function as chaperone proteins for expression and translocation of active matriptase and hepsin to the cell surface (32) (Fig. 2*B*), as well as ANTXR1 and ANTXR2 (Fig. 2*C*), which are receptors required for PAS cell surface binding. Importantly, cell surface serine protease activity was significantly increased in all of the OvCa cell lines compared to nontumorigenic IOSE397 cells (Fig. 2*D* and *SI Appendix*, Fig. S1*E*), confirming the overactivity of tumor-associated MASPs compared to their regulated state in nontumorigenic cells.

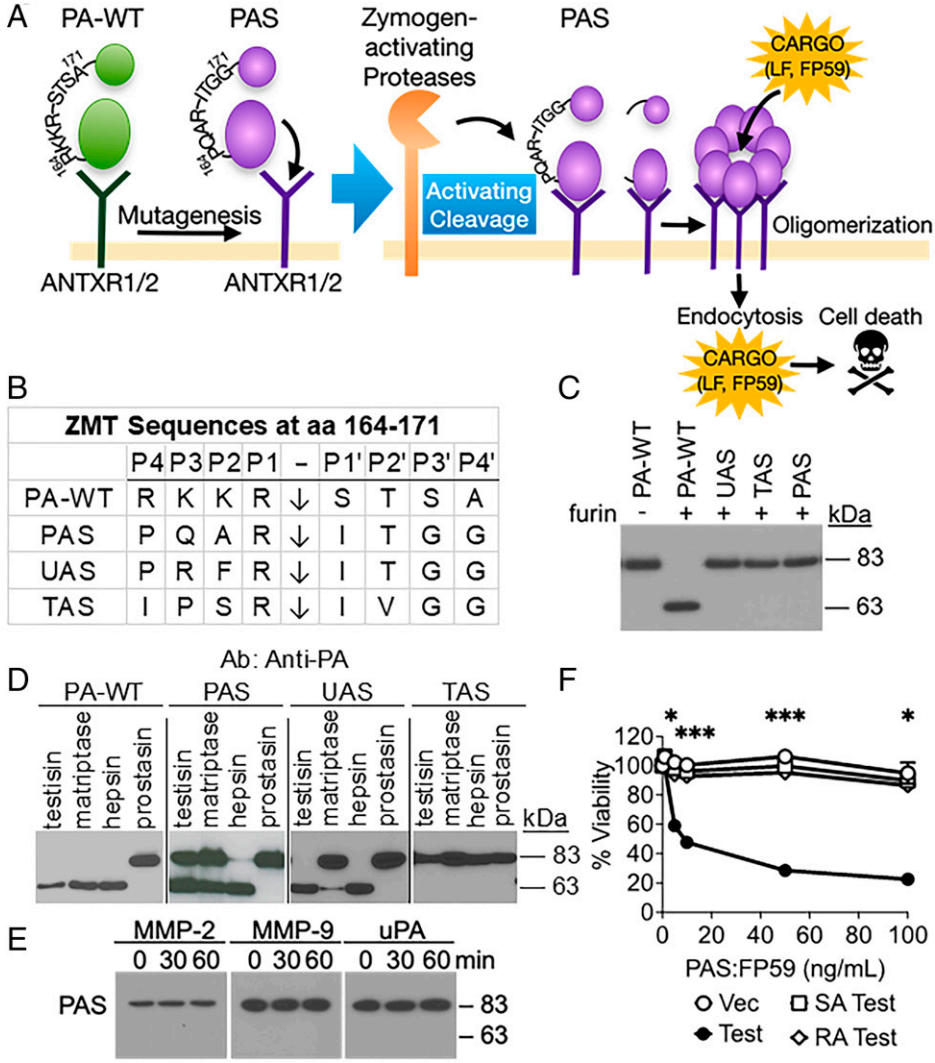

Fig. 1. Generation and characterization of ZMT proteins. (*A*) ATs exert their cytotoxic actions in a three-step activation process that involves a) the binding of PA to surface receptors on target cells, b) the translocation of cytotoxic cargo proteins to the cytoplasmic compartment of the target cells, and c) the induction of cell death by cytotoxins in the cytoplasm (16). Initiation occurs by the binding of PA to either of two ubiquitously cell surface–expressed receptors, tumor endothelial marker-8 (TEM-8, ANTXR1) or capillary morphogenesis protein-2 (CMG-2, ANTXR2) (17). Following binding of PA to its receptors, PA-WT activation cleavage by furin catalyzes the formation of an oligomeric pore that enables highly efficient protease-activated delivery of cytotoxic cargo proteins (e.g., LF, FP59) into the cytosol (18–23). The ZMTs (e.g., UAS, TAS, and PAS) are produced by mutation of the furin activation sequence, which abrogates furin activation and confers activation by pericellular zymogen-activating proteases. Proteolytic cleavage must occur on the cell surface to achieve activation of the catalytic PA. (*B*) ZMT activation cleavage sequences of wild-type (PA-WT) and mutant PA proteins UAS, TAS, and PAS. The peptide bond is cleaved after the arginine residue in the P1 position, indicated by a vertical arrow. The lysine in the P1 position of the native uPA zymogen activation site was substituted with an arginine residue in order to make the sequence a predicted better substrate for hepsin and matriptase (13). (*C*) ZMTs were no longer cleaved by recombinant furin when incubated for 2.5 h at 30 °C. Cleavage products were detected by immunoblotting using an anti-PA polyclonal antibody, detecting inactive full-length PAS (83 kDa) and the cleaved activated form of PAS (63 kDa). (*D*) Cleavage of purified PA-WT and ZMTs by MASPs. Recombinant PA-WT and ZMTs were incubated with the soluble protease domains of testisin, matriptase, hepsin, and prostasin (50 nM) for 2.5 h. (*E*) Time course of PAS incubation with recombinant MMP-2, MMP-9, and uPA for 30 and 60 min. ((*F*) Active testisin is required for PAS:FP59–induced cytotoxicity. HEK293T cells were transiently transfected with vector alone (Vec), wild-type testisin (Test), catalytically inactive mutant testisin (SA-Test), or zymogen-locked mutant testisin (RA-Test). At 48 h after transfection, cells were incubated with PAS (0 to 100 ng/mL):FP59 (50 ng/mL) for 6 h, medium was replaced, and viability was measured by MTT assay after 48 h. Data represent the average of two independent experiments ± SEM performed in triplicate (*$P < 0.05$, ***$P < 0.005$). aa, amino acid; Ab, antibody.

PAS Toxin-Induced Antitumor Cytotoxicity Requires Serine Protease Activity. The generality of PAS activation and toxin-induced ovarian tumor cell killing was investigated by treatment of the panel of OvCa cell lines with PAS:FP59 (Fig. 2*E*). The results showed variable cytotoxicity in all OvCa cell lines (Fig. 2*E*). To evaluate the requirement of MASP cleavage for PAS:FP59 cytotoxicity, ES-2 and NCI/ADR-Res cells were pre-incubated with the synthetic serine protease inhibitor AEBSF prior to PAS:FP59 treatment. AEBSF pretreatment resulted in significant attenuation of toxicity in both cell lines (Fig. 2*F*), confirming that PAS:FP59 toxin-induced killing specifically requires MASP activity.

Although the nontumorigenic IOSE397 cells displayed low cell surface serine protease activity (Fig. 2*D*), they were highly susceptible to killing by PAS:FP59 (Fig. 2*E* and *SI Appendix*, Fig. S2*A*; EC_{50}, 4 ng/mL). While delivery of FP59 is a useful reporter for evaluating proteolytic cleavage of PAS in in vitro tumor cell cultures, even delivery of small amounts of FP59 from low-level PAS activation causes potent translation inhibition and cell death. FP59 is toxic in vivo, since only 2 μg FP59 in combination with native PA is sufficient to kill a mouse (17). The natural AT cargo, LF, is ∼50-fold less potent than FP59 (17) and functions by a different, more selective mechanism of inhibiting prosurvival signaling pathways commonly

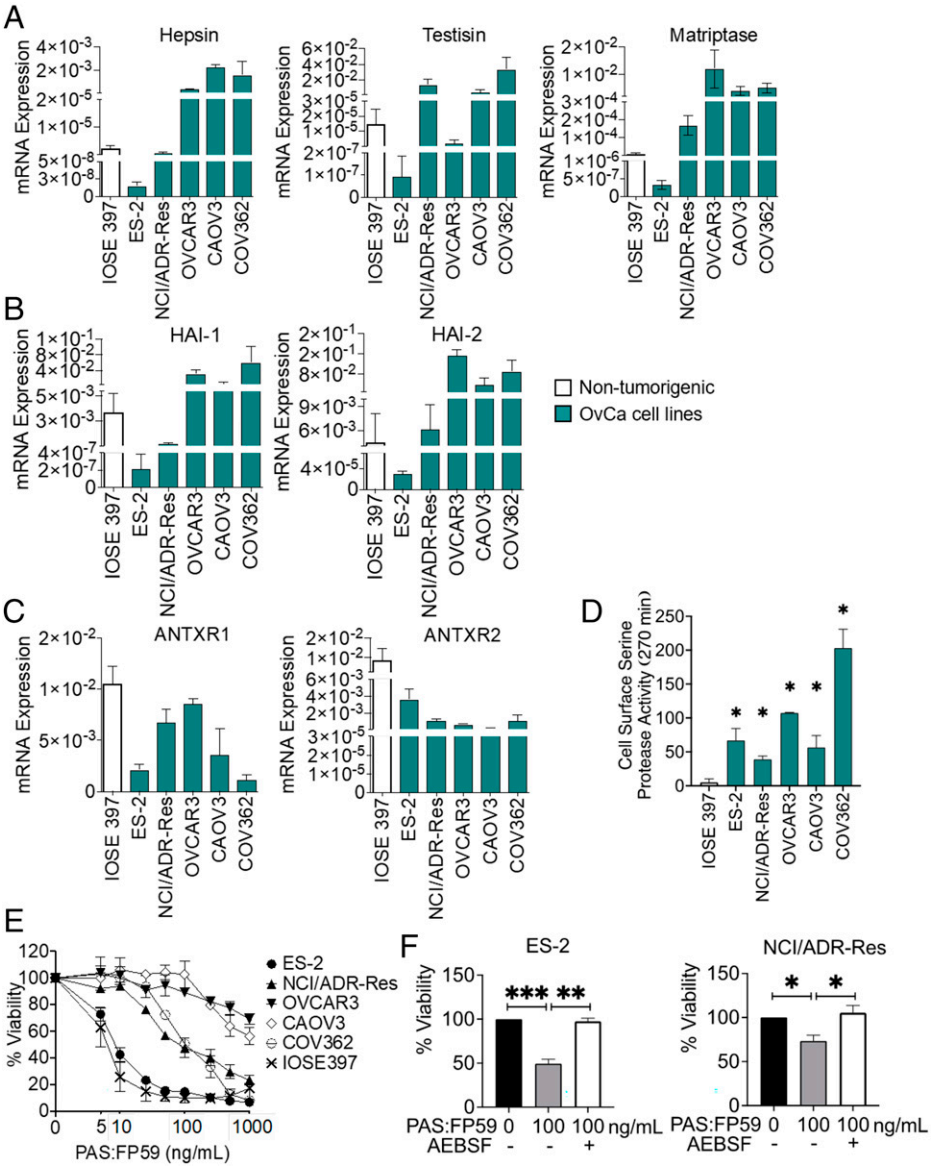

Fig. 2. Ovarian tumor cells possess the machinery for sensitivity to PAS toxin. Comparison of messenger RNA (mRNA) expression among five OvCa cell lines and the nontumorigenic control IOSE397. (*A–C*) mRNA expression of (*A*) MASPs hepsin, testisin, and matriptase, (*B*) HAI-1 and HAI-2, and (*C*) ANTXR1 (TEM-8) and ANTXR2 (CMG-2) was determined by qPCR analysis. Data are represented as $2^{-\Delta CT}$ relative to glyceraldehyde-3-phosphate dehydrogenase (GAPDH) and is the average ± SEM from two independent experiments performed in triplicate. (*D*) Comparison of cell surface serine protease activity measured by fluorogenic peptide cleavage assay. Cell lines were incubated with Boc-QAR-AMC (100 μM) without or with AEBSF for 270 min (*Left Panel*). End point values at 270 min (*Right Panel*). Data represent the average of triplicate values ± SEM from two to three independent experiments (*$P < 0.05$ relative activity to IOSE397). (*E*) OvCa cell lines and IOSE397 were treated with the indicated concentrations of PAS:FP59, and cell viability was measured by MTT assay after 48 h. Data represent average viability ± SEM from two to three independent experiments performed in triplicate. (*F*) Inhibition of cell surface serine protease activity attenuates PAS:FP59 cytotoxicity in ES-2 and NCI/ADR-Res cells. Cells were incubated without or with AEBSF (100 μM) for 30 min, then treated with PAS:FP59 (0 or 100 ng/mL) for 4 h, and medium was replaced. Cell viability was determined after 48 h by MTT assay. Treatment with AEBSF alone caused some cell toxicity (75 to 98%) depending on the experiment. The data were normalized to untreated cells and corrected for toxicity of AEBSF alone. Data represent an average viability ± SEM of three independent experiments performed in triplicate (*$P < 0.05$, **$P < 0.01$, ***$P < 0.005$).

utilized by tumor cells. Treatment with PAS:LF was cytotoxic to ES-2 cells (Fig. 3*A* and *SI Appendix*, Fig. S2*A*; EC_{50}, 158 ng/mL). Cytotoxicity was attenuated by AEBSF protease inhibition, showing dependence of PAS:LF on MASP activity (Fig. 3*A*). Notably, IOSE397 cells were not affected by treatment with PAS:LF (Fig. 3*B* and *SI Appendix*, Fig. S2*A*; EC_{50} > 1,000 ng/mL).

The multidrug-resistant NCI/ADR-Res cells were resistant to PAS:LF (Fig. 3*B* and *SI Appendix*, Fig. S2*A*; EC_{50} > 1,000 ng/mL); however, we found that multiple sequential treatments of PAS:LF enhanced cell killing. (Fig. 3*B*). ES-2 cells showed increased cytotoxicity with multiple sequential treatments of PAS:LF, while multiple treatments did not affect IOSE397 cells (Fig. 3*B*), suggesting that optimization of dosing regimens with PAS:LF can further enhance antitumor cytotoxicity. Treatment of these cell lines with LF alone did not induce cytotoxicity under the same conditions (*SI Appendix*, Fig. S2*B*), confirming that the PAS:LF toxin requires both components for antitumor toxicity. Together, these data indicate that PAS:LF is a promising strategy for tumor cell selective cytotoxicity.

Susceptibility of OvCa Monolayers and Spheroids to PAS:LF Cytotoxicity. Because OvCa cells are frequently found in the peritoneal cavity as spheroids and since spheroid formation can alter the properties of tumor cells to promote drug resistance

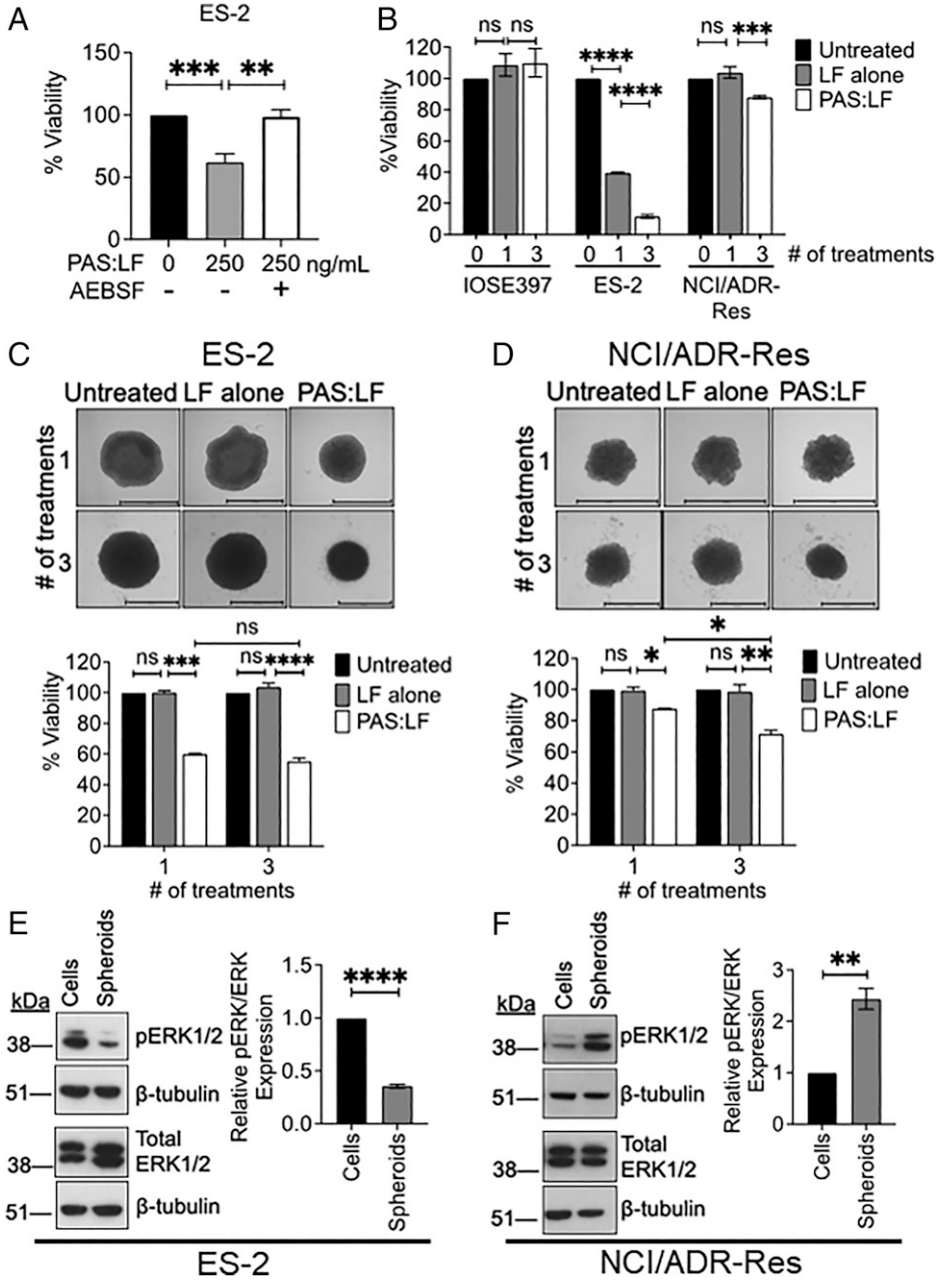

Fig. 3. Susceptibility of OvCa cell lines and spheroids to PAS:LF toxin. (*A*) Inhibition of cell surface serine protease activity with AEBSF attenuates PAS:LF cytotoxicity in ES-2 cells. ES-2 cells were incubated without or with AEBSF (100 μM) for 30 min, then treated with PAS:LF (0 or 250 ng/mL) for 4 h, and medium was replaced. Cell viability was determined after 48 h by MTT assay. Data represent an average viability ± SEM of three independent experiments performed in triplicate (***P* < 0.01, ****P* < 0.005). (*B*) ES-2 and NCI/ADR-Res cells were treated with PAS:LF (1,000 ng/mL) one time or three times every 48 h, and cell viability was measured by MTT assay after 48 h. Data represent an average of three to five replicate values ± SEM from three to five independent experiments (****P* < 0.005, *****P* < 0.001; ns, not significant). (*C* and *D*) Susceptibility of OvCa spheroids to PAS:LF toxin. (*C*) ES-2 and (*D*) NCI/ADR-Res spheroids were formed on agarose-coated 96-well plates overnight and then treated with 1,000 ng/mL LF alone or PAS:LF one time or three times every 48 h. Spheroid viability was measured 48 h after the last treatment by PrestoBlue or ImageJ quantification of decrease in size. Data represent average viability of two or three independent experiments ± SEM performed in triplicate (**P* < 0.05, ***P* < 0.01, ****P* < 0.005, *****P* < 0.001; ns, not significant). (*E* and *F*) Whole-cell lysates prepared from (*E*) ES-2 and (*F*) NCI/ADR-Res cells and spheroids were analyzed by sodium dodecyl sulfate–polyacrylamide gel electrophoresis (SDS PAGE) and immunoblotted for human anti-phosphorylated extracellular signal-related kinase (pERK1/2) and total ERK1/2 on separate Western blots (rabbit monoclonal antibodies, Cell Signaling Technologies); β-tubulin was probed on each blot as an independent loading control (rabbit polyclonal antibody, Santa Cruz Biotechnologies) (*Left Panels*). Signals quantitated by densitometry (ImageJ) were normalized to β-tubulin and represented as relative pERK/total ERK (average of values from three independent experiments ± SEM. ***P* < 0.01, *****P* < 0.001) (*Right Panels*).

(33), we investigated the susceptibility of multicellular ovarian tumor spheroids to PAS:LF toxin. Spheroids were generated in vitro using ES-2 and NCI/ADR-Res cells by plating them on low-attachment agarose-coated plates. PAS:LF achieved a 40 to 45% reduction in viability of ES-2 spheroids when treated either once or three sequential times over a 7-d period (Fig. 3*C*). Although monolayer NCI/ADR-Res cells were resistant to one treatment of PAS:LF, NCI/ADR-Res spheroids showed an ∼15% reduction in viability after one treatment and an ∼30% reduction in viability after three sequential treatments (Fig. 3*D*). Similar to cell monolayers, both ES-2 and NCI/ADR-Res spheroids were sensitive to treatment with PAS:FP59 (*SI Appendix*, Fig. S2*C*), confirming effective PAS cleavage. These data demonstrate the antitumor effect of PAS:LF in OvCa spheroids and

suggest differences between monolayers and formed spheroids in their susceptibility to PAS:LF cytotoxicity.

Differential Susceptibility of OvCa Monolayers and Spheroids to PAS:LF Cytotoxicity Correlates with MAPK Pathway Activation. Since LF irreversibly inactivates MEKs (24, 25), we compared the activation status of endogenous pERK1/2 levels in ES-2 and NCI/ADR-Res monolayers and formed spheroids, which could contribute to their different susceptibilities to PAS:LF. High levels of pERK1/2 were detected in the ES-2 monolayers, which were significantly decreased in spheroids formed from the ES-2 cells (Fig. 3*E*). On the other hand, minimal ERK1/2 activation was detected in the NCI/ADR-Res monolayers, but pERK1/2 was substantially increased in the formed NCI/ADR-Res spheroids (Fig. 3*F*). Total ERK1/2 levels were similar between the monolayers and spheroids for both cell lines (Fig. 3 *E* and *F*). These data suggest that there is plasticity in MAPK pathway activation between cancer cell monolayers and formed spheroids and that increased MAPK pathway activation likely influences increased susceptibility to PAS:LF–induced killing.

Potent Antitumor Effect of PAS:LF Toxin on a Preclinical Orthotopic ES-2–Luc Xenograft Model of OvCa Dissemination and Metastasis. The ability of PAS:LF toxin to inhibit OvCa tumor growth and metastasis in vivo was initially investigated using an established intraperitoneal (i.p.) ES-2–Luc orthotopic xenograft model (34), which reproduces key events of late-stage OvCa dissemination and metastasis. Cohorts of female athymic nude mice were injected i.p. with ES-2–Luc cells, and tumor burden was monitored longitudinally in live animals using the in vivo imaging system (IVIS). After 4 d, tumor-bearing mice were sorted into four cohorts (5 mice/group), and each cohort received four total i.p. injections composed of -15 μg PAS:5 μg LF, 15 μg PAS alone, 5 μg LF alone, or vehicle (phosphate-buffered saline [PBS]) twice a week for 2 wk; mice were euthanized on day 15 (Fig. 4 *A*, *i*). Mice treated with PAS:LF showed significantly reduced tumor burden over the course of the experiment (Fig. 4 *A*, *ii*), and after 15 d, the average tumor burden in PAS:LF–treated mice measured just 3% of the tumor burden present in vehicle alone (PBS)–treated mice (Fig. 4 *A*, *iii*). In mice treated with PBS, PAS, or LF alone, ES-2–Luc tumor burden appeared as widespread small tumor foci that were too numerous to count. These tumor nodules were distributed throughout the abdominal cavity, both floating in the ascites as spheroids and attached to various organs and the peritoneal wall. The tumor foci favored attachment adjacent to blood vessels of the tissue layer lining the peritoneal cavity, as well as membranous tissue surrounding the mesenteric arteries located in between—and distributing blood to—the intestinal tract (Fig. 4 *A*, *iv*). Tumors were consistently observed to accumulate on the diaphragm as a thick white layer of tumor cell plaque covering the translucent muscle. Tumor foci were distributed adjacent to the spleen, liver, kidneys, and intestinal tract. Disease presentation in this model is consistent with disease presentation in OvCa patients (35). In contrast, PAS:LF–treated mice did not present with ascites fluid accumulation or widespread tumor foci throughout the peritoneal cavity (Fig. 4 *A*, *iv*). All treatments of the PAS:LF toxin or the components alone were well tolerated, as the mice experienced no treatment-specific weight loss, adverse symptoms, or gross organ damage as visualized upon necropsies. These data demonstrate that PAS:LF toxin effectively reduces OvCa dissemination and metastasis in vivo. Coadministration of both PAS and LF is required for effective killing, showing that cytotoxicity is not due to the action of either component alone.

PAS:LF Toxin Extends Survival of ES-2–Luc Tumor-Bearing Mice. To determine the effect of PAS:LF on mouse longevity, cohorts of mice bearing ES-2–Luc tumors were treated with three doses of PAS:LF or vehicle alone (PBS). The disease was allowed to progress until the mice reached experimental end points (Fig. 4 *B*, *i*). Tumor-bearing mice treated with all doses of PAS:LF displayed significantly reduced tumor burden (Fig. 4 *B*, *ii*) and lived significantly longer (1.7- to 2-fold increased survival) (Fig. 4 *B*, *iii*) compared with mice treated with vehicle. Upon euthanasia, mice treated with vehicle alone had significant tumor dissemination throughout the peritoneal cavity similar to Fig. 4 *A*, *iv*. These data demonstrate that the PAS:LF treatment significantly prolonged the mean survival time of mice compared to control animals ($P < 0.001$).

Potent Antitumor Effect of PAS:LF Toxin on Advanced Disease. In view of the limited treatment options for the majority of patients with advanced-stage OvCa, we sought to determine the antitumor effect of PAS:LF on established peritoneal metastases. Ten days after i.p. injection with ES-2–Luc ovarian tumor cells, when significant tumor burden was established, mice received i.p. injections of two different doses of PAS:LF or vehicle alone (PBS) (Fig. 4 *C*, *i*). There were only two treatments in total because tumor growth proceeded rapidly in mice treated with vehicle alone. In vivo imaging showed that while tumor burden was significant and widespread in vehicle-treated mice, the mice treated with both doses of PAS:LF showed significantly reduced tumor burden with just two treatments (Fig. 4 *C*, *ii*). The average tumor burden in PAS:LF–treated mice measured ∼28% and 20% of the tumor burden present in vehicle-treated mice, respectively (Fig. 4 *C*, *iii*). These mice also presented with fewer tumor nodules on the diaphragm and on the mesenteric arteries during necropsies (Fig. 4 *C*, *iv*). These data demonstrate the efficacy of PAS:LF treatment against advanced OvCa.

Proteolytic Activation Is Required for PA to Reduce ES-2–Luc Tumor Burden. To assess the requirement of proteolytic activation for the PAS:LF toxin to kill ES-2–Luc tumor cells in vivo, the antitumor effect of PAS was compared with that of a mutant PA protein, PA-U7 (36), that was designed to not be cleaved by any known proteases (^{164}PQAR replaced with ^{164}PGG). Mice bearing ES-2–Luc tumors were injected i.p. with PAS:LF, PA-U7:LF, or PBS (Fig. 5 *A*, *i*). Tumor burden was significantly abrogated in cohorts treated with PAS:LF relative to mice treated with either PA-U7 or PBS (Fig. 5 *A*, *i* and *ii*). Mice treated with PAS:LF toxin possessed only 2.6% of the tumor burden of vehicle-treated mice and 2% of the tumor burden of PA-U7–treated mice on day 11 (Fig. 5 *A*, *ii*). Upon necropsy, PAS:LF–treated mice showed substantially reduced tumors around the mesenteric arteries and on the diaphragm compared with mice treated with vehicle or PA-U7 toxin, similar to Fig. 4 *A*, *iv*. All treatments were well tolerated. These data show that the PA system is highly selective and requires proteolytic activation for its antitumor effect in vivo.

PAS:LF Toxin Treatment Reduces Ovarian Tumor Burden in a Second Orthotopic Xenograft Model of OvCa Metastasis: NCI/ADR-Res–Luc. To address the generality of the PAS:LF antitumor effect, we developed a second model of i.p. dissemination and metastasis using NCI/ADR-Res–Luc cells originally derived from a high-grade serous adenocarcinoma. NCI/ADR-Res–Luc

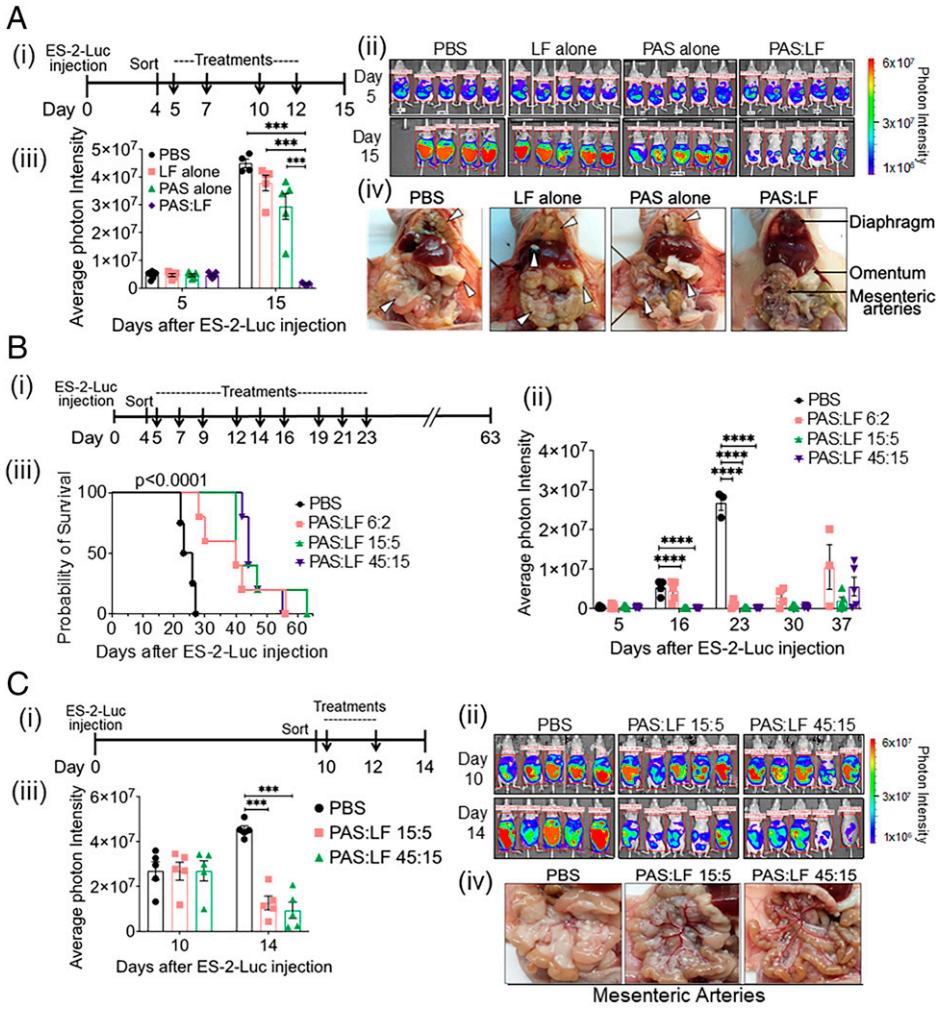

Fig. 4. PAS:LF toxin effectively reduces tumor burden and extends survival in preclinical xenograft models. (*A*) ES-2–Luc orthotopic model of OvCa dissemination and metastasis. (*i*) At Day 0, female athymic nude mice (5/group) were injected i.p. with 5×10^6 ES-2–Luc cells (400 μL) and sorted 4 d later according to equal tumor burden. Cohorts of mice were treated with vehicle alone (PBS), 5 μg LF alone, 15 μg PAS alone, or 15 μg PAS:5 μg LF at Day 5 and twice a week thereafter (indicated by arrows) until euthanized on day 14. Tumor burden was measured via IVIS imaging periodically. (*ii*) Images represent the peak luciferase activity levels in the individual mice monitored by in vivo bioluminescence imaging. (*iii*) Quantification of the average photon intensity ± SEM (***$P <$ 0.005). (*iv*) Representative images upon necropsy show tumor burden completely covering the diaphragm in PBS-, LF alone–, and PAS alone–treated mice, while diaphragms of PAS:LF–treated mice remain transparent enough to see the lungs underneath. Tumor burden in PBS-, LF alone–, and PAS alone–treated mice completely obstructs the mesenteric arteries, whereas the arteries are visible in PAS:LF toxin–treated mice. Representative tumor nodules on the diaphragm, liver, omentum, and mesenteric arteries are highlighted by white arrowheads. (*B*) Survival analysis. (*i*) Female athymic nude mice were injected with 5×10^6 ES-2–Luc cells (i.p.) at day 0, and tumors were allowed to develop for 4 d with tumor burden monitored by IVIS. Mice were sorted into cohorts with equal tumor burden (5 mice/group) on day 4 and then were treated on day 5 with either vehicle (PBS) or increasing doses of PAS:LF toxin (6 μg PAS:2 μg LF, 15 μg PAS:5 μg LF, or 45 μg PAS:15 μg LF) three times per week for 3 wk (indicated by arrows). Mice were weighed three times per week, and metastatic disease was allowed to progress until mice reached experimental end points or succumbed to the disease. The experiment was terminated on day 63, with one mouse in the 15 μg PAS:5 μg LF group showing no disease. (*ii*) Quantification of the average photon intensity ± SEM of the peak luciferase activity levels over time monitored in the individual mice on IVIS imaging (****$P <$ 0.001). (*iii*) Kaplan-Meier survival analysis was generated using GraphPad Prism software, and significance was tested by log-rank (Mantel-Cox) test (****$P <$ 0.0001 among all four groups, **$P = 0.0027$ for each treatment group compared to vehicle control group). (*C*) ES-2–Luc model of advanced stage OvCa. (*i*) Female athymic nude mice were injected with 5×10^6 ES-2–Luc cells (i.p.), and tumors developed for 10 d. Mice sorted into cohorts with equal tumor burden (5/group) were treated with vehicle (PBS), 15 μg PAS:5 μg LF, or 45 μg PAS:5 μg LF on Day 10. Mice were treated twice (as indicated by arrows) and euthanized on day 14. (*ii*) Tumor burden was monitored over time by IVIS imaging. (*iii*) Average photon intensity ± SEM was quantified (***$P <$ 0.005). (*iv*) Upon necropsy, mesenteric arteries are visible in both cohorts of PAS:LF–treated mice, whereas the mesenteric arteries are obstructed by tumor burden in PBS control mice.

metastases develop more slowly than ES-2–Luc metastases in vivo, but the pattern of tumor burden is similar to that of ES-2–Luc (*SI Appendix*, Fig. S3). Cohorts of female athymic nude mice bearing NCI/ADR-Res–Luc tumors were treated with two doses of PAS:LF or LF alone (Fig. 5 *B*, *i*). Quantification of tumor burden by IVIS imaging showed that by day 25 after tumor injection, treatment with PAS:LF resulted in a 67% reduction in NCI/ADR-Res–Luc tumor burden at the lower dose tested and a 74% reduction at the higher dose compared to LF alone (Fig. 5 *B*, *ii*). The maximal reduction in tumor burden was achieved with 45 μg PAS:15 μg LF when the experiment was terminated, an almost 90% reduction in tumor burden compared to treatment with LF alone (Fig. 5 *B*, *ii*). These data further demonstrate the significant efficacy of PAS:LF treatment in preclinical models of OvCa.

PAS:LF Toxin Treatment Reduces Ovarian Tumor Burden in an ES-2–Luc Minimal Residual Disease Model of OvCa Metastasis. Currently, the standard treatment for advanced OvCa is debulking surgery to reduce tumor size to less than 1 cm followed by postoperative chemotherapy (37), with most women also undergoing a bilateral salpingo-oophorectomy with hysterectomy.

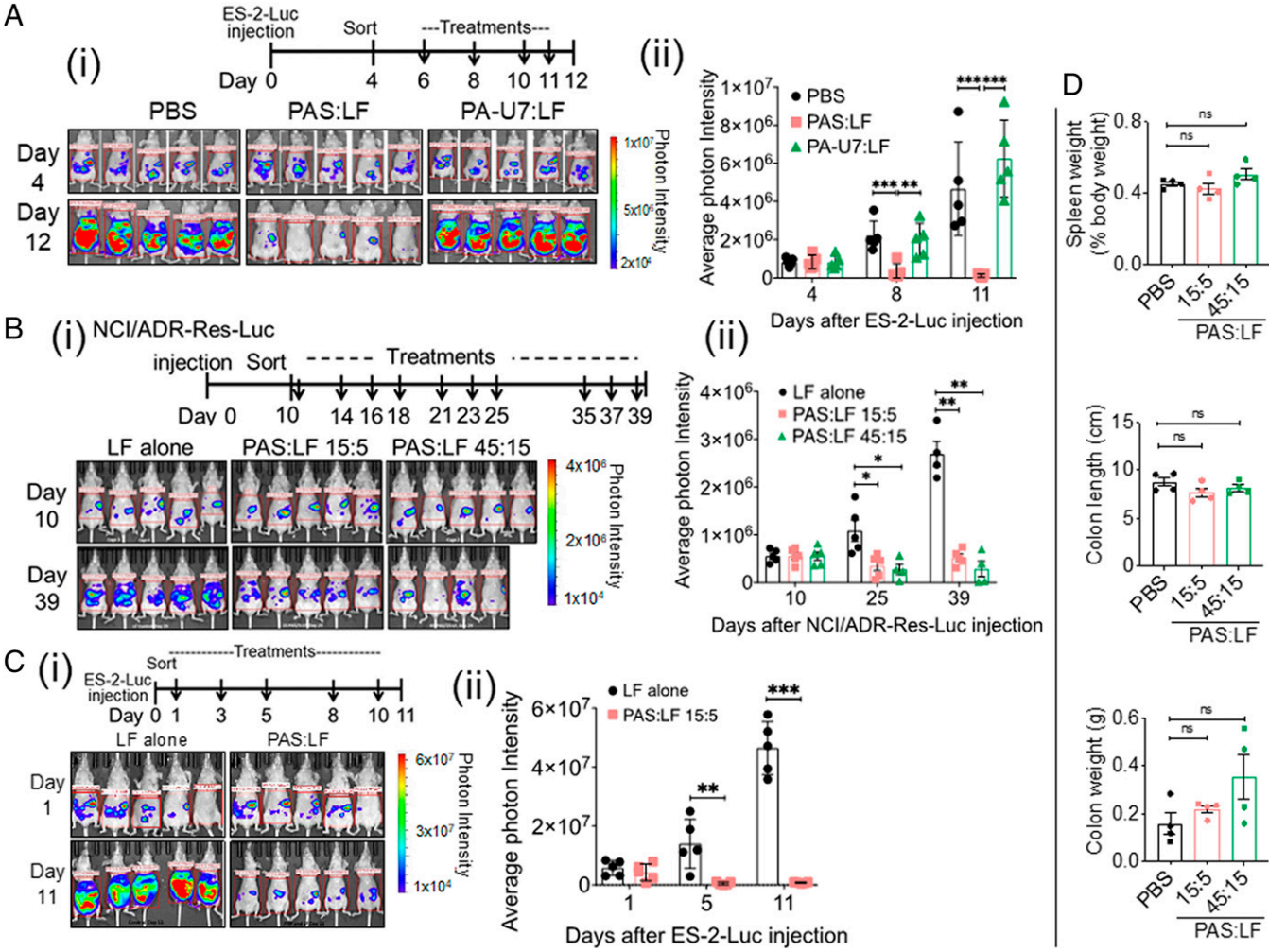

Fig. 5. PAS:LF toxin requires proteolytic activation; reduces tumor burden in a second orthotopic xenograft model, NCI/ADR-Res-Luc; is effective in ovariectomized mice; and is well tolerated in mice. (*A*) PAS:LF toxin requires proteolytic activation for its antitumor effect in vivo. (*i*) Four days after i.p. injection of 5×10^6 ES-2–Luc cells, female nude mice (5/group) were treated with 5 μg LF alone, 15 μg PAS:5 μg LF, or 15 μg PA-U7:5 μg LF for a total of four doses (indicated by arrows) and were euthanized on day 12. (*ii*) Tumor burden was monitored over time by IVIS imaging. Average photon intensity ± SEM was quantified (**$P < 0.01$, ***$P < 0.005$). (*B*) NCI/ADR-Res–Luc orthotopic model of ovarian tumor dissemination and metastasis. (*i*) Cohorts of female athymic nude mice were injected i.p. with 5×10^6 NCI/ADR-Res–Luc cells and 10 d after injection were sorted into three cohorts with similar tumor burden (5 mice/group) as measured by IVIS imaging. Each cohort received three i.p. injections every week over 4 wk (indicated by arrows) containing 15 μg PAS:5 μg LF, 45 μg PAS:15 μg LF, or 5 μg LF alone. (*ii*) Tumor burden was monitored at days 10, 25, and 39 after tumor injection by IVIS imaging. Images represent the peak luciferase activity levels. One mouse in the 45:15 PAS:LF group was euthanized due to body weight loss after day 10. Photon intensities via IVIS imaging are quantified; data are represented as mean ± SEM (*$P < 0.05$, **$P < 0.01$). (*C*) PAS:LF toxin effectively reduces tumor burden in an ES-2–Luc minimal residual disease model of OvCa. (*i*) Ovariectomized nude mice were injected i.p. with 5×10^6 ES-2–Luc cells, and the following day mice were imaged using IVIS and sorted into two cohorts (5 mice/group) with similar tumor burden. PAS:LF treatment (15 μg PAS:5 μg LF or 5 μg LF alone) was initiated at day 1 after tumor injection, when tumor burden was barely detectable to replicate minimal disease. The cohorts received a total of five treatments over 2 wk (indicated by arrows). (*ii*) Tumor burden was monitored at days 1 and 11 by IVIS imaging. Mice were euthanized on day 11 due to advanced tumor burden and accumulation of ascites in the LF control group. Average photon intensity was quantified ± SEM (**$P < 0.01$, ***$P < 0.005$). (*D*) PAS:LF toxin was well tolerated in mice. Female CD1 mice (4/group) were treated with i.p. injections of vehicle (PBS) or escalating doses of PAS:LF (15 μg PAS:5 μg LF or 45 μg PAS:15 μg LF) three times a week for 2 wk. Upon necropsy, spleen weight, empty colon length, and empty colon weight were recorded as signs of gross inflammation or toxicity. Complete blood counts, blood chemistries, and histological analyses are provided in *SI Appendix*, Fig. S5. Data represent four mice per group ± SEM (ns, nonsignificant).

However, tumor recurrence can stem from minimal residual disease remaining following surgery and development of chemoresistance. To investigate the efficacy of PAS:LF in reducing residual tumors postsurgery, we established a minimal residual disease xenograft model using ovariectomized female nude mice. Mice were injected i.p. with ES-2–Luc cells and the following day were treated with PAS:LF or LF alone, when tumor burden was barely detectable (Fig. 5 *C*, *i*) to replicate minimal disease. Quantification of IVIS imaging revealed that treatment with PAS:LF toxin resulted in a rapid and significant decrease in tumor burden by day 5, with PAS:LF–treated mice showing a 97% reduction in tumor burden compared to those treated with LF alone; this growth inhibition was effectively maintained throughout the treatments (Fig. 5 *C*, *ii*). These data provide evidence that PAS:LF toxin is effective in reducing residual tumors after debulking surgery.

PAS:LF Toxin Treatment Is Well Tolerated in Mice. Administration of PAS:LF elicits robust in vivo antitumor responses and appears to be well tolerated in several diverse models of advanced OvCa. To investigate potential PAS:LF toxicities at effective antitumor doses used in the xenograft OvCa models, outbred CD1 mice were challenged with PAS:LF15:5, PAS:LF 45:15, or vehicle alone (PBS) delivered i.p. three times per week for 2 wk. The appearance, movement, and behavior of all mice remained normal throughout the experimental period. Complete necropsies were performed after 2 wk, including

gross overall inspection, histopathological studies, and blood chemistry analysis. We found that the treatments that gave effective antitumor responses in the xenograft tumor models were well tolerated as judged by no significant effects on spleen weights, colon lengths, and colon weights (Fig. 5*D*). Since PAS has the potential to be activated by MASPs expressed in various tissues, as confirmed by BioGPS Database analysis (*SI Appendix*, Fig. S4), we also analyzed potential off-target organs (liver, kidney, and colon) by histopathological analyses. No significant structural damage was observed, and overall blood count and chemical analysis showed no apparent toxicities (*SI Appendix*, Fig. S5). These data confirmed that the PAS:LF toxin is well tolerated at the effective doses used in vivo.

PAS:LF Toxin Impairs Growth of Tumor Cells from Patient-Derived Ascites. Because tumor cell lines can acquire unanticipated phenotypes during adaptation to in vitro culture conditions, we sought to investigate PAS:LF efficacy in primary human OvCa. Examination of hepsin, matriptase, and testisin gene expression using a Human Ovarian Cancer TissueScan Array demonstrated that these MASPs are significantly elevated in OvCa across different histological types and stages compared to normal ovarian tissue (Fig. 6*A*). Tumor cells in ascites are a major source of disease recurrence in OvCa patients (5). To investigate the susceptibility of primary human tumor cells to PAS:LF cytotoxicity, ascites fluid from OvCa patients representing different stages, origins, and subtypes was collected, and cytospins were stained to confirm expression of key identifiers of ovarian tumor cells, CA125 and PAX8 (Fig. 6*B*). The tumor cells were cultured on low-attachment agarose, where they formed organotypic multicellular spheroids within 24 h. Treatment with PAS:LF (2 to 6 μg/mL) resulted in ∼40% reduced tumor cell viability; similarly, treatment with PAS:FP59 resulted in ∼48% reduced tumor viability across these heterogeneous patient specimens (Fig. 6 *C*, *i* and *ii*) and *SI Appendix*, Fig. S6 *A* and *B*). These data suggest that PAS:LF toxin is likely to be broadly effective for a wide range of OvCa patients.

PAS:LF Toxin Impairs the Growth of Ovarian PDXs. PDX models have the advantage of preserved fidelity to the original cancer in terms of genomic characteristics and retention of intratumoral heterogeneity. Chemoresistant epithelial ovarian PDX tumors implanted subcutaneously (s.c.) into the flanks of female NRG mice were treated intratumorally with PAS:LF,

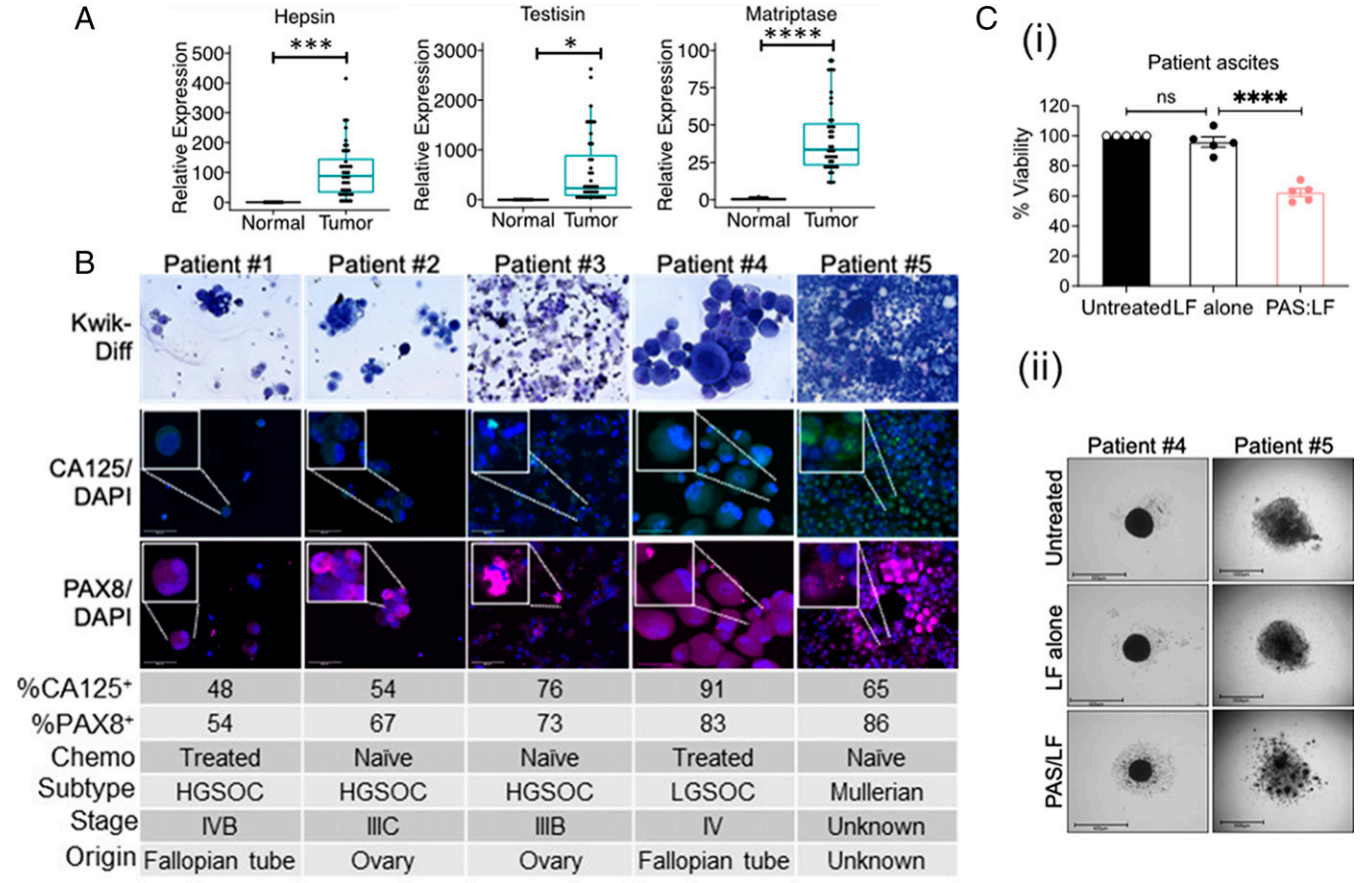

Fig. 6. Potent antitumor cytotoxicity of PAS:LF toxin in patient-derived primary human tumors. (*A*) Real-time qPCR analysis showing increased hepsin, testisin, and matriptase mRNA expression in patients with OvCa of various histological type and stage of tumorigenic development (Human Ovarian Cancer TissueScan Array; Origene) compared with normal ovary tissue. Data are representedin box plots showing the median, lower and upper quartiles (horizontal lines) of relative expression ±SEM compared to normal ovary tissue normalized to β-actin (*$P < 0.05$, ***$P < 0.005$, ****$P < 0.001$). (*B*) Tumor cells recovered from ascites fluids from five patients were collected by centrifugation, contaminating red blood cells were removed by hypotonic lysis, and cytospins were assessed for tumor purity by Kwik-Diff stain and expression of the OvCa markers CA125 and PAX8. Images are 40X original magnification. Insets are close-up images of individual cells or clusters. The tumor cell percentage of total cells in ascites fluid was quantified using ImageJ. The chemotherapy (Chemo) treatment status, histological subtype, tumor stage, and primary tumor origin were determined by independent staff pathologists as part of the clinical diagnosis. HGSOC, high-grade serous ovarian carcinoma; LGSOC, low-grade serous ovarian carcinoma. (*C*) (*i*) The recovered human ascites tumor cells were seeded on agarose-coated plates for 24 h, where they formed organotypic multicellular spheroids. Spheroids that were treated twice with PAS:LF (Patients #1 and #2: 2 μg/mL, Patients #3 to #5: 6 μg/mL) for a total of 120 h. Spheroid viability relative to untreated controls was quantified via PrestoBlue or ImageJ quantification of decrease in size and is shown as an average of the five patient samples ± SEM performed in three to six replicates (****$P < 0.001$; ns, not significant). (*ii*) Representative images of spheroids from Patient #4 and Patient #5 after 120 h of treatment are shown. Scale bars = 650μm.

LF alone, PAS alone, or vehicle (PBS) (Fig. 7 *A*, *i*). The tumors treated with vehicle, PAS alone, or LF alone were significantly larger than the tumors treated with PAS:LF by day 27 (4.7-, 4.5-, and 3-fold, respectively) ($P < 0.001$) (Fig. 7 *A*, *ii* and *iii*). In an independent experiment, cohorts of mice carrying ovarian PDX tumors were treated with i.p. injections of PAS:LF or LF alone (Fig. 7 *B*, *i*). By day 20, the tumors treated with LF alone grew significantly to an approximate fourfold increase in volume, whereas no significant increase was observed in PAS:LF–treated tumors (only about a 1.3-fold difference in volume ($P < 0.005$) (Fig. 7 *B*, *ii* and *iii*). Histopathological analysis of hematoxylin/eosin(H&E)–stained tumor tissues following the intratumoral (*SI Appendix*, Fig. S7*A*) and i.p. (Fig. 7*C*) treatments showed that the antitumor effects occurred predominantly through necrosis. Histopathological analyses of potential off-target organs showed no significant structural damage

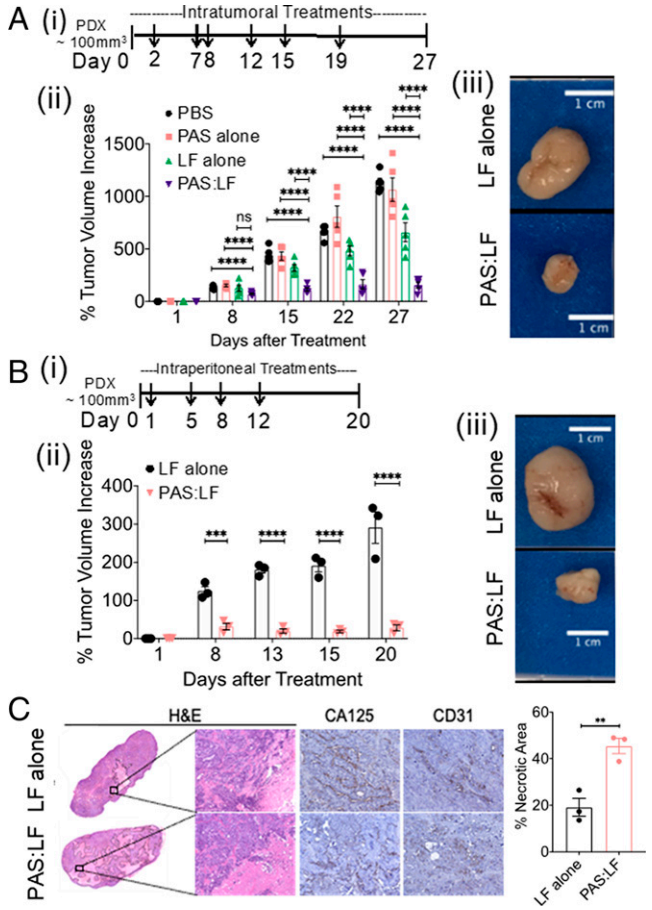

Fig. 7. PAS:LF toxin reduces tumor burden in a PDX model of OvCa and is well tolerated in mice. The human ovarian PDX tumor (NCI:572874–153-T) was implanted and expanded in female NRG mice, then injected s.c. into three to five mice per treatment group. (*A*) Once tumors reached ~100 mm^3, (*i*) mice were treated with a total of 6 intratumoral injections (as indicated by arrows) of vehicle (PBS), 5 μg LF alone, 15 μg PAS alone, or 15 μg PAS:5 μg LF (5/group) over ~3 wk. (*ii*) Tumor volumes were measured using calipers over time (****$P < 0.001$; ns, nonsignificant). Error bars represent SEM. (*iii*) Tumors were harvested at end point (representative images of harvested tumors are shown). (*B*) (*i*) PDX tumors were also treated with a total of four i.p. injections (indicated by arrows) of 5 μg LF alone or 15 μg PAS:5 μg LF (3/group) over 1.5 wk. (*ii*) Tumor volumes were measured using calipers over time (***$P < 0.005$, ****$P < 0.001$). Error bars represent SEM. (*iii*) Tumors were harvested at end point (representative images of harvested tumors are shown). (*C*) Harvested tumors treated with i.p. doses were paraffin embedded, sectioned, and H&E stained (representative images of 10X whole scan and 20X magnified area) (*Left Panel*). Serial sections were stained with CA125 and CD31. Percent necrotic area was quantified from H&E whole scans using ImageJ; data represent average values from three mice/group ± SEM (**$P < 0.01$ *Right Panel*).

(*SI Appendix*, Fig. S7*B*). These data demonstrate a potent antitumor effect of the PAS:LF toxin on a human patient tumor in a mouse model in vivo, by direct or clinically relevant indirect delivery.

Discussion

Here, we describe the development of a protease-activated, AT-based prodrug that exploits the hyperactivity and overexpression of tumor-associated, zymogen-activating serine proteases, which are recognized as modulating the metastatic properties of these tumors. PAS:LF kills OvCa cells in vitro and substantially inhibits dissemination and metastasis of OvCa in i.p. xenograft models as well as ovarian PDX tumor models, with no apparent adverse effects on normal tissues. These data indicate that PAS:LF toxin is a strong candidate for further translational development.

Proteases have been an attractive target in cancer research due to their roles in tumor growth and metastasis (38). Protease inhibitors designed to block activity, however, have generally resulted in a nonselective inhibition profile or systemic toxicity (39), indicating the need for better therapeutic approaches to target tumor-associated protease hyperactivity. Harnessing the catalytic power of tumor-associated proteases with protease-activated prodrugs designed to deliver cytotoxins is currently showing promise for combining target site activation with selective delivery and specificity (39). The PAS:LF toxin is based on an AT delivery system reengineered into a prodrug requiring zymogen-activating serine proteases in the tumor pericellular environment for selective antitumor cytotoxicity. Zymogen activation is a very tightly regulated enzymatic process that is expected to be relatively unaffected by PAS:LF in normal settings. In the tumor microenvironment, however, PAS serves as a potent substrate for hyperactive proteases. The irreversible nature of proteolytic cleavage allows these tumor-associated serine proteases to act as unidirectional switches. The multicomponent aspect of PAS:LF–induced cytotoxicity requires several steps to occur (e.g., PAS cell surface binding, proteolytic activation, endocytosis, delivery of cytotoxic cargoes, and dependence on active MAPK survival signaling for LF) and requires several additional factors (e.g., ANTXR1/2 expression, inhibitor expression), further enhancing selectivity and reducing off-target activation.

OvCa is a heterogeneous disease consisting of several different subtypes, which are likely to express varying ZMT-activating proteases depending on tumor biology and functional requirements. The ability of multiple zymogen-activating serine proteases with overlapping substrate specificities to activate the PAS:LF toxin confers an advantage for its antitumor effects, since the toxin will remain effective if a tumor cell evades treatment by downregulating an individual MASP or inhibiting its enzymatic activity. PAS was not cleaved by widely expressed furin, prostasin, uPA, or MMP-2/-9 (Fig. 1 *D* and *E*), which implies that this toxin is likely to be specifically activated with minimal off-target activation by proteases with broad normal physiological functions. The lack of any visible side effects or organ damage upon necropsy after in vivo treatments with PAS:LF strengthens this notion.

The sensitivity of ES-2 and NCI/ADR-Res cells and spheroids to PAS:LF appeared to be correlated with ERK1/2 activation, supporting the notion that MAPK pathway activation is a possible determinant of tumor susceptibility to PAS:LF–induced killing. OvCa is characterized by oncogenic driver mutations, several of which induce ERK1/2 activation. These include p53 (particularly in the high-grade serous subtype), *BRCA1/2*,

KRAS, *NF1*, *CDK12*, *PIK3CA*, and *BRAF*, all of which have roles in the regulation of the Ras-MAPK-MEK-ERK1/2 signaling pathway (40–43). The most common *BRAF* mutation, V600E, contributes synergistically to constitutive MAPK function and predicts sensitivity to MEK inhibitors as it positively correlates with increased pERK1/2 levels (44, 45). ES-2 cells, which are highly responsive to PAS:LF cytotoxicity, contain the V600E mutation and show substantial pERK1/2 expression (Fig. 3*E*). Thus, *RAS* or *BRAF* mutation status and pERK1/2 levels could predict sensitivity to PAS:LF cytotoxicity. Recent clinical studies indicate that BRAF inhibition in combination with MAPK inhibitors (e.g., trametinib or cobimetinib) results in enhanced therapeutic efficacy (44). However, these and other similar MEK inhibitors are reversible and have a low therapeutic index, which causes off-target effects and short-lived responses. PAS:LF could be a tumor-selective enzymatic alternative that irreversibly directly cleaves and inactivates MAPK signaling pathway components and thus would be potentially more efficient compared to MEK inhibitors currently under investigation.

The Ras-Raf-MEK-ERK1/2 pathway is dysregulated in almost 40% of all human cancers, likely due to mutations in *BRAF* (~10%) and its upstream activator *RAS* (~30%) (46). This suggests that PAS:LF may be an effective strategy for targeting other cancers characterized by constitutive activation of these prosurvival pathways [e.g., prostate (47), lung (48), pancreatic (49), and breast (50)]. Hepsin, matriptase, and other MASPs are hyperactive in several of these tumors (7), providing a similarly attractive pericellular microenvironment for PAS:LF activation and tumor killing.

In summary, we provide strong evidence that the engineered AT mechanism that utilizes overactive MASPs is a promising translational therapeutic approach to improve the outlook of women diagnosed with advanced OvCa. This study revealed that testisin, hepsin, or matriptase can be targeted with an engineered AT to kill OvCa tumor cells in vitro and in vivo as well as human ascites-derived OvCa tumor cells, which play a dominant role in OvCa disease recurrence (51). Our preclinical data show that PAS:LF toxin-induced killing is tumor specific without obvious adverse effects, which strongly suggests potential efficacy as an antitumor therapy with minimal side effects once a safe dose is determined.

Materials and Methods

Additional materials and methods are described in *SI Appendix*.

Mutagenesis and Purification of ZMTs. Two-step overlap PCR mutagenesis was used to replace the P4-P4′ furin cleavage site in the PA expression plasmid pYS5-PA33 with the sequences listed in Fig. 1*B*. Recombinant ZMTs and LF proteins were expressed using *B. anthracis* strain BH480 and purified as described previously (52). For cleavage assays, ZMTs (1 μM) were incubated with recombinant proteases (50 nM) for indicated intervals.

Cell Culture. ES-2, OVCAR3, CaOV3, and COV362 cell lines were purchased from American Type Culture Collection, and NCI/ADR-Res cells were from the National Cancer Institute Division of Cancer Treatment and Diagnosis repository. IOSE397 (immortalized ovarian surface epithelial cells) were obtained from the Canadian Ovarian Tissue Bank (University of British Columbia, Vancouver, Canada).

Cell and Spheroid Cytotoxicity Assays. Viability of cells treated with PAS:LF (0 ng/mL to 1,000 ng/mL) or PAS:FP59 (0 ng/mL to 1,000 ng/mL) at equal concentrations (molar ratios: PAS:LF 1:0.92; PAS:FP59 1:1.4) for 48 h after one treatment or after three sequential treatments every 48 h was assessed by MTT assay (Invitrogen), and absorbance was measured using a FlexStation 3 spectrophotometer (Thermo Fisher Scientific). Spheroids formed on 0.75% agarose coating overnight were treated with PAS:LF or PAS:FP59 (0 ng/mL to 5,000 ng/mL) once for 48 h or every 48 h over a period of 7 d and were imaged by the EVOS FL Auto Cell Imaging System (Life Technologies). Viability was assessed by measuring the circumference of the treated and untreated spheroids (ImageJ) and/or by PrestoBlue (Thermo Fisher Scientific).

Fluorogenic Peptide Cleavage Assay. Cells were incubated with 100 μM Boc-QAR-AMC peptide (R&D Systems) in Opti-MEM I in the absence or presence of the serine protease inhibitor AEBSF (100 μM). Peptide cleavage and release of the 7-amino-4-methylcoumarin (AMC) group was monitored at excitation 380 nm and emission 460 nm.

Animal Studies. ES-2–Luc cells were described previously (34), and stable NCI/ADR-Res–Luc cells were generated in a similar fashion. Female athymic nude (Nu/Nu) mice (6 to 8 wk) or ovariectomized mice were purchased from Envigo. ES-2–Luc or NCI/ADR-Res–Luc cells (5×10^6 in 400 μL) were administered i.p.; tumor burden was monitored using the in vivo imaging system (IVIS-Xenogen). Mice with similar photon intensity were sorted into cohorts of 5 mice/group and injected i.p. with the indicated treatments. Tumor burden was assessed by IVIS weekly or biweekly. For PDX studies, female *NOD.Cg-Rag1 < tm1Mom> Il2rg < tm1Wjl>/SzJ* (NRG) mice (Jackson Laboratories) were injected s.c. with the human OvCa PDX tumor line NCI:572874–153-T (NCI PDMR) and treated with i.p or intratumoral PAS:LF toxin (3 to 5 mice/group). Tumor volume was measured weekly by electronic calipers. For toxicity studies, female CD1 outbred mice ($n = 4$/group) were challenged with i.p. injections of PBS or two doses of PAS:LF three times a week for 2 wk. Upon euthanasia of all animal experiments, liver, kidney, colon, and tumors were collected and fixed in 4% paraformaldehyde (PFA) for histopathological analyses. All animal experiments were conducted in compliance with Public Health Service (PHS) guidelines for animal research and were approved by the University of Maryland Baltimore Institutional Animal Care and Use Committee.

Isolation of Human OvCa Cells from Ascites Fluid. De-identified patient tumor cells and ascites fluids were used in this study. Tissues were recovered at the time of surgery in excess of pathology requirements with informed consent under protocol GCC1488. This study was approved by the Institutional Review Board of the University of Maryland, Baltimore, MD. Ascites fluid was centrifuged, the supernatant preserved, and the cellular contents isolated after red blood cell lysis. Immunofluorescence staining for CA125 and PAX8 of cytospin preparations confirmed OvCa cell purity. Organotypic multicellular spheroids were formed on agarose-coated plates and subjected to PAS toxin treatment; viability was assessed as above.

Data Availability. The sequences reported in this paper have been deposited in the GenBank database: PAS, accession number LQ782047.1, (53); UAS, accession no. LQ782049.1, (54); TAS, accession no. LQ782045.1, (55); and PA-WT, accession no. LQ782063.1, (56). All other data are included in the article and/or *SI Appendix*.

ACKNOWLEDGMENTS. We thank the patients who generously provided tissues for these studies. The authors thank Eun Yong Choi, Kayla Tighe, and Xinrong Ma of the University of Maryland Marlene and Stewart Greenebaum Comprehensive Cancer Center Translational Laboratory Shared Service for assistance with xenograft models of OvCa and Tierra Johnson and Jathiya Bailey for assistance with toxicology experiments with CD1 mice. This work was supported in part by NIH Grants R01 CA196988 (T.M.A.) and R01 HL118390 (T.M.A.), the Mary Kay Ash Foundation (T.M.A.), NCI, Cancer Center Support Grant P30CA134274, the Maryland Department of Health's Cigarette Restitution Fund Program (R.G.L., J.R., and T.M.A.), the NIH intramural research program of the National Institute of Allergy and Infectious Diseases (S.L. and S.H.L.), NIH Grant R01 CA254938 (S.L.), and an Institutional Research Grant IRG-16-123-13 award from the American Cancer Society (M.S.B.). N.R.P. was supported by an NIH T32 Training Grant in Cancer Biology fellowship (T32CA154274), and E.W.M. was supported by an NIH T32 Integrative Training Program in Membrane Biology fellowship (T32GM008181). J.R. and D.M.R. are supported by Department of Obstetrics, Gynecology and Reproductive Sciences departmental grants. T.M.A. is an employee of the Veterans Affairs Maryland Health Care System. The views reported in this paper do not reflect the views of the Department of Veterans Affairs or the United States Government.

Author affiliations: [a]Center for Vascular and Inflammatory Diseases, University of Maryland School of Medicine, Baltimore, MD 21201; [b]Department of Physiology, University of Maryland School of Medicine, Baltimore, MD 21201; [c]Marlene and Stewart

Greenebaum Comprehensive Cancer Center, University of Maryland School of Medicine, Baltimore, MD 21201; [d]National Institute of Allergy and Infectious Diseases, NIH, Bethesda, MD 20892; [e]Obstetrics, Gynecology and Reproductive Sciences, University of Maryland School of Medicine, Baltimore, MD 21201; and [f]Research & Development Service, VA Maryland Health Care System, Baltimore, MD 21201

Author contributions: N.D., N.R.P., E.W.M., G.D.C., R.G.L., S.L., S.H.L., and T.M.A. designed research; N.D., N.R.P., E.W.M., M.S.B., G.D.C., and R.G.L. performed research; E.W.M., S.L., J.R., G.G.R., D.M.R., S.H.L., and T.M.A. contributed new reagents/analytic tools; N.D., N.R.P., E.W.M., M.S.B., G.D.C., S.L., and T.M.A. analyzed data; and N.D., N.R.P., M.S.B., and T.M.A. wrote the paper.

1. D. D. Bowtell *et al.*, Rethinking ovarian cancer II: Reducing mortality from high-grade serous ovarian cancer. *Nat. Rev. Cancer* **15**, 668–679 (2015).
2. S. Arora *et al.*, FDA approval summary: Olaparib monotherapy or in combination with bevacizumab for the maintenance treatment of patients with advanced ovarian cancer. *Oncologist* **26**, e164–e172 (2021).
3. K. S. Tewari *et al.*, Final overall survival of a randomized trial of bevacizumab for primary treatment of ovarian cancer. *J. Clin. Oncol.* **37**, 2317–2328 (2019).
4. M. Sait Bakir *et al.*, Bevacizumab in recurrent ovarian cancer. *J. BUON* **26**, 1271–1278 (2021).
5. E. Lengyel, Ovarian cancer development and metastasis. *Am. J. Pathol.* **177**, 1053–1064 (2010).
6. N. Thomakos *et al.*, Rare distant metastatic disease of ovarian and peritoneal carcinomatosis: A review of the literature. *Cancers (Basel)* **11**, E1044 (2019).
7. N. R. Pawar, M. S. Buzza, T. M. Antalis, Membrane-anchored serine proteases and protease-activated receptor-2-mediated signaling: Co-conspirators in cancer progression. *Cancer Res.* **79**, 301–310 (2019).
8. M. Vizovisek, D. Ristanovic, S. Menghini, M. G. Christiansen, S. Schuerle, The tumor proteolytic landscape: A challenging frontier in cancer diagnosis and therapy. *Int. J. Mol. Sci.* **22**, 2514 (2021).
9. O. Vasiljeva, E. Menendez, M. Nguyen, C. S. Craik, W. Michael Kavanaugh, Monitoring protease activity in biological tissues using antibody prodrugs as sensing probes. *Sci. Rep.* **10**, 5894 (2020).
10. R. Oliveira-Silva *et al.*, Monitoring proteolytic activity in real time: A new world of opportunities for biosensors. *Trends Biochem. Sci.* **45**, 604–618 (2020).
11. A. P. Soleimany *et al.*, Activatable zymography probes enable *in situ* localization of protease dysregulation in cancer. *Cancer Res.* **81**, 213–224 (2021).
12. M. J. Whitley *et al.*, A mouse-human phase 1 co-clinical trial of a protease-activated fluorescent probe for imaging cancer. *Sci. Transl. Med.* **8**, 320ra4 (2016).
13. T. M. Antalis, M. S. Buzza, K. M. Hodge, J. D. Hooper, S. Netzel-Arnett, The cutting edge: Membrane-anchored serine protease activities in the pericellular microenvironment. *Biochem. J.* **428**, 325–346 (2010).
14. T. H. Bugge, T. M. Antalis, Q. Wu, Type II transmembrane serine proteases. *J. Biol. Chem.* **284**, 23177–23181 (2009).
15. C. E. Martin, K. List, Cell surface-anchored serine proteases in cancer progression and metastasis. *Cancer Metastasis Rev.* **38**, 357–387 (2019).
16. C. Bachran, S. H. Leppla, Tumor targeting and drug delivery by anthrax toxin. *Toxins (Basel)* **8**, 197 (2016).
17. S. Liu, Y. Zhang, B. Hoover, S. H. Leppla, The receptors that mediate the direct lethality of anthrax toxin. *Toxins (Basel)* **5**, 1–8 (2012).
18. J. P. Hobson, S. Liu, S. H. Leppla, T. H. Bugge, Imaging specific cell surface protease activity in living cells using reengineered bacterial cytotoxins. *Methods Mol. Biol.* **539**, 115–129 (2009).
19. S. H. Leppla, N. Arora, M. Varughese, Anthrax toxin fusion proteins for intracellular delivery of macromolecules. *J. Appl. Microbiol.* **87**, 284 (1999).
20. C. Bachran *et al.*, Cytolethal distending toxin B as a cell-killing component of tumor-targeted anthrax toxin fusion proteins. *Cell Death Dis.* **5**, e1003 (2014).
21. C. Bachran *et al.*, Anthrax toxin-mediated delivery of the *Pseudomonas* exotoxin A enzymatic domain to the cytosol of tumor cells via cleavable ubiquitin fusions. *MBio* **4**, e00201-13 (2013).
22. X. Liao, A. E. Rabideau, B. L. Pentelute, Delivery of antibody mimics into mammalian cells via anthrax toxin protective antigen. *ChemBioChem* **15**, 2458–2466 (2014).
23. W. P. Verdurmen, M. Luginbühl, A. Honegger, A. Plückthun, Efficient cell-specific uptake of binding proteins into the cytoplasm through engineered modular transport systems. *J. Control. Release* **200**, 13–22 (2015).
24. N. S. Duesbery *et al.*, Proteolytic inactivation of MAP-kinase-kinase by anthrax lethal factor. *Science* **280**, 734–737 (1998).
25. A. J. Bardwell, M. Abdollahi, L. Bardwell, Anthrax lethal factor-cleavage products of MAPK (mitogen-activated protein kinase) kinases exhibit reduced binding to their cognate MAPKs. *Biochem. J.* **378**, 569–577 (2004).
26. N. Arora, K. R. Klimpel, Y. Singh, S. H. Leppla, Fusions of anthrax toxin lethal factor to the ADP-ribosylation domain of *Pseudomonas* exotoxin A are potent cytotoxins which are translocated to the cytosol of mammalian cells. *J. Biol. Chem.* **267**, 15542–15548 (1992).
27. S. Liu, S. H. Leppla, Retroviral insertional mutagenesis identifies a small protein required for synthesis of diphthamide, the target of bacterial ADP-ribosylating toxins. *Mol. Cell* **12**, 603–613 (2003).
28. V. M. Gordon, K. R. Klimpel, N. Arora, M. A. Henderson, S. H. Leppla, Proteolytic activation of bacterial toxins by eukaryotic cells is performed by furin and by additional cellular proteases. *Infect. Immun.* **63**, 82–87 (1995).
29. E. W. Martin *et al.*, Targeting the membrane-anchored serine protease testisin with a novel engineered anthrax toxin prodrug to kill tumor cells and reduce tumor burden. *Oncotarget* **6**, 33534–33553 (2015).
30. S. Domcke, R. Sinha, D. A. Levine, C. Sander, N. Schultz, Evaluating cell lines as tumour models by comparison of genomic profiles. *Nat. Commun.* **4**, 2126 (2013).
31. E. J Devor, J. R Lapierre, D. P Bender, ES-2 Ovarian Cancer Cells Present a Genomic Profile Inconsistent with their Reported History. *Obstet. Gynecol. Res.* **04**, (2021).
32. H. Kataoka, M. Kawaguchi, T. Fukushima, T. Shimomura, Hepatocyte growth factor activator inhibitors (HAI-1 and HAI-2): Emerging key players in epithelial integrity and cancer. *Pathol. Int.* **68**, 145–158 (2018).
33. S. Al Habyan, C. Kalos, J. Szymborski, L. McCaffrey, Multicellular detachment generates metastatic spheroids during intra-abdominal dissemination in epithelial ovarian cancer. *Oncogene* **37**, 5127–5135 (2018).
34. G. D. Conway *et al.*, PRSS21/testisin inhibits ovarian tumor metastasis and antagonizes proangiogenic angiopoietins ANG2 and ANGPTL4. *J. Mol. Med. (Berl.)* **97**, 691–709 (2019). Correction in: *J. Mol. Med. (Berl.)* **97**, 1375 (2019).
35. R. L. Coleman, B. J. Monk, A. K. Sood, T. J. Herzog, Latest research and treatment of advanced-stage epithelial ovarian cancer. *Nat. Rev. Clin. Oncol.* **10**, 211–224 (2013).
36. S. Liu, T. H. Bugge, S. H. Leppla, Targeting of tumor cells by cell surface urokinase plasminogen activator-dependent anthrax toxin. *J. Biol. Chem.* **276**, 17976–17984 (2001).
37. D. Wang, G. Zhang, C. Peng, Y. Shi, X. Shi, Choosing the right timing for interval debulking surgery and perioperative chemotherapy may improve the prognosis of advanced epithelial ovarian cancer: A retrospective study. *J. Ovarian Res.* **14**, 49 (2021).
38. L. Sevenich, J. A. Joyce, Pericellular proteolysis in cancer. *Genes Dev.* **28**, 2331–2347 (2014).
39. M. Poreba, Protease-activated prodrugs: Strategies, challenges, and future directions. *FEBS J.* **287**, 1936–1969 (2020).
40. M. Burotto, V. L. Chiou, J. M. Lee, E. C. Kohn, The MAPK pathway across different malignancies: A new perspective. *Cancer* **120**, 3446–3456 (2014).
41. S. R. Whittaker *et al.*, A genome-scale RNA interference screen implicates NF1 loss in resistance to RAF inhibition. *Cancer Discov.* **3**, 350–362 (2013).
42. H. Liu, K. Liu, Z. Dong, Targeting CDK12 for cancer therapy: Function, mechanism, and drug discovery. *Cancer Res.* **81**, 18–26 (2021).
43. R. J. Kurman, Origin and molecular pathogenesis of ovarian high-grade serous carcinoma. *Ann. Oncol.* **24** (suppl. 10), x16–x21 (2013).
44. M. P. Campos *et al.*, *BRAF* mutations occur infrequently in ovarian cancer but suggest responsiveness to BRAF and MEK inhibition. *JCO Precis. Oncol.* **2**, PO.18.00025 (2018).
45. N. Nakayama *et al.*, *KRAS* or *BRAF* mutation status is a useful predictor of sensitivity to MEK inhibition in ovarian cancer. *Br. J. Cancer* **99**, 2020–2028 (2008).
46. S. Lee, J. Rauch, W. Kolch, Targeting MAPK signaling in cancer: Mechanisms of drug resistance and sensitivity. *Int. J. Mol. Sci.* **21**, E1102 (2020).
47. B. Georgi *et al.*, Evolving therapeutic concepts in prostate cancer based on genome-wide analyses (review). *Int. J. Oncol.* **45**, 1337–1344 (2014).
48. J. Han *et al.*, MEK inhibitors for the treatment of non-small cell lung cancer. *J. Hematol. Oncol.* **14**, 1 (2021).
49. E. A. Collisson *et al.*, A central role for RAF→MEK→ERK signaling in the genesis of pancreatic ductal adenocarcinoma. *Cancer Discov.* **2**, 685–693 (2012).
50. K. S. Saini *et al.*, Targeting the PI3K/AKT/mTOR and Raf/MEK/ERK pathways in the treatment of breast cancer. *Cancer Treat. Rev.* **39**, 935–946 (2013).
51. A. Latifi *et al.*, Isolation and characterization of tumor cells from the ascites of ovarian cancer patients: Molecular phenotype of chemoresistant ovarian tumors. *PLoS One* **7**, e46858 (2012).
52. A. P. Pomerantsev *et al.*, A *Bacillus anthracis* strain deleted for six proteases serves as an effective host for production of recombinant proteins. *Protein Expr. Purif.* **80**, 80–90 (2011).
53. N. Duru *et al.*, Engineered anthrax protective antigen proteins for cancer therapy. NCBI. https://www.ncbi.nlm.nih.gov/nuccore/LQ782047.1. Deposited 27 June 2018.
54. N. Duru *et al.*, Engineered anthrax protective antigen proteins for cancer therapy. NCBI. https://www.ncbi.nlm.nih.gov/nuccore/LQ782049.1. Deposited 27 June 2018.
55. N. Duru *et al.*, Engineered anthrax protective antigen proteins for cancer therapy. NCBI. https://www.ncbi.nlm.nih.gov/nuccore/LQ782045.1. Deposited 27 June 2018.
56. N. Duru *et al.*, Engineered anthrax protective antigen proteins for cancer therapy. NCBI. https://www.ncbi.nlm.nih.gov/nuccore/LQ782063.1. Deposited 27 June 2018.